HOKKAIDO UNIVERSITY

Title	Development of electrostatic-induced charge detector for multiturn time-of-flight mass spectrometer
Author(s)	Bajo, Ken-ichi; Aoki, Jun; Ishihara, Morio; Furuya, Shizuho; Nishimura, Masahiro; Yoshitake, Miwa; Yurimoto, Hisayoshi
Citation	Journal of Mass Spectrometry, 57(11), e4892 https://doi.org/10.1002/jms.4892
Issue Date	2022-11-22
Doc URL	http://hdl.handle.net/2115/90847
Rights	This is the peer reviewed version of the following article: Bajo, K, Aoki, J, Ishihara, M, et al. Development of electrostatic-induced charge detector for multiturn time-of-flight mass spectrometer. J Mass Spectrom. 2022; 57(11):e4892., which has been published in final form at https://doi.org/10.1002/jms.4892. This article may be used for non-commercial purposes in accordance with Wiley Terms and Conditions for Use of Self-Archived Versions. This article may not be enhanced, enriched or otherwise transformed into a derivative work, without express permission from Wiley or by statutory rights under applicable legislation. Copyright notices must not be removed, obscured or modified. The article must be linked to Wiley's version of record on Wiley Online Library and any embedding, framing or otherwise making available the article or pages thereof by third parties from platforms, services and websites other than Wiley Online Library must be prohibited.
Type	article (author version)
File Information	J. Mass Spectrom._57(11)_e4892.pdf

Development of electrostatic-induced charge detector for multiturn time-of-flight mass spectrometer

Short title
Development of non-destructive ion detector for multiturn TOF–MS

Ken-ichi Bajo[1] [*], Jun Aoki[2, 3, 4], Morio Ishihara[2], Shizuho Furuya[5], Masahiro Nishimura[5], Miwa Yoshitake[5] and Hisayoshi Yurimoto[1, 5]

[1] Department of Earth and Planetary Sciences, Hokkaido University, Sapporo, Japan

[2] Department of Physics, Graduate School of Science, Osaka University, Toyonaka, Japan

[3] Graduate School of Frontier Biosciences, Osaka University, Suita, Japan

[4] Riken Center for Biosystems Dynamics Research, Kobe, Japan

[5] ISAS/JAXA, Sagamihara, Japan

[*] Corresponding author. E-mail: k-bajo@eis.hokudai.ac.jp   Tel.: +81 11 706 9174.

Keywords: multiturn TOF–MS, electrostatic-induced charge detector, MULTUM, non-destructive ion detection, mass assignment

1   Abstract

2   We developed an autocorrelation function to resolve the overtaking problem in
3   a multiturn time-of-flight mass spectrometer (TOF–MS). The function analyzes the
4   characteristic period for one lap of each ion packet and derives a mass spectrum from a
5   signal pulse train composed of multiturn ion packets. To detect the ion pulse train, a new
6   non-destructive ion detector was developed and installed in the multiturn orbit of
7   MULTUM-S II. This detector is composed of an electrostatically induced charge detector,
8   a preamplifier, and a digitizer. The electrostatic noises are smaller than the single-ion
9   signals owing to the accumulation of the multiturn TOF spectrum. The conventional ion
10   detector of TOF–MS is operated after collecting the signal pulse train. The multiturn TOF
11   spectrum was convolved with an autocorrelation function to derive the mass spectrum.
12   The convolved mass spectrum performed a mass resolving power (MRP) of 28,200 at m/z
13   69 and mass accuracy of 28 ppm for the perfluorotributylamine (PFTBA) gas sample.

14

1. Introduction

Multiturn ion optics with perfect space and time focusing were developed to achieve infinite mass resolving power (MRP) time-of-flight mass spectrometry.[1] The optics were installed in time-of-flight mass spectrometers (TOF–MS), MULTUM, and MULTUM II, which provide ultra-high MRP to attain an $M/\Delta M = 6 \times 10^5$.[2-8] The optics also dramatically reduce the size of TOF–MS.

Although the optics provided ultra-high MRP with a compact MS, it introduced the so-called overtaking problem for the mass spectrum, in which ions having small m/z overtake ions having large m/z when the flight time (pass length) is increased.[9] As a result, the time-of-flight (TOF) spectrum after the flight is not aligned according to m/z. When many ion species with different m/z simultaneously fly in the multiturn trajectory, the overtaking ions complicate the TOF spectrum. This characteristic makes the universal use of multiturn TOF–MS difficult, and the applications may be restricted to a narrow range of m/z in the multiturn trajectory.[10,11] In this study, we traced every multiturn ion using a novel electrostatic-induced charge detector (iCD) installed in multiturn optics. We analyzed the overtaking problem of the multiturn TOF spectrum using an autocorrelation function to derive the mass spectrum.

2. Electrostatic-induced charge detector (iCD)

An electron impact (EI) type TOF–MS, infiTOF (MSI. TOKYO, Inc., Japan), equipped with MULTUM-S II was used.[9, 12] An iCD was installed in the ion optics of the MULTUM-S II (Figure 1a).

A stainless steel tube with an inner diameter of 6 mm and a length of 18 mm was used to make the iCD. The iCD connects the input gate electrode of a field-effect transistor to a charge-sensitive preamplifier (CSA) A250CF CoolFET® (Amptek Inc., USA) (Figure 1b). The iCD is shielded by an exterior body at ground potential. The iCD was set in the multiturn ion optics between the electrostatic sectors of the MULTUM-S II (Figure 1a). The electrostatic-induced charges caused by a multiturn ion packet were detected by the iCD. When an ion packet with positive charges (+Q) passes through the iCD, charges −Q and +Q are induced on the inner and outer surfaces of the iCD, respectively. The +Q charges can be measured using CSA without any effect on the ion packet (Figure 1b). The output voltage is 0.64 μV when a single charged ion passes through the iCD.

3. Data acquisition system

A schematic illustrating the data acquisition system for the electrostatic-induced

charge detection is shown in Figure 2. This system resembles that of the data acquisition system reported by Bajo et al.[13] The pulse signals from the A250CF preamplifier are converted into 10-bits digital signals using the NI PXIe-5160 (5160) digitizer. The sampling rate and voltage resolution are 104.167×10^6 samples s^{-1} and 48.8 μV (10-bits and ± 0.025V for peak-to-peak voltage), respectively. Streaming data processing and recording are performed using the NI PXIe-8880 (8880) as a controller of the PXI-platform (National Instruments corp., USA). This system is controlled using the LabVIEW program.

The 10-bits digital signals are converted into 16-bits iCD spectrum, and then multiplied and subtracted by the gain and the offset of 5160 digitizer settings, respectively. The arbitrary repetitive acquisition data for the iCD spectra are converted into 64-bits double precision floating point numbers and averaged. The acquisition data are stored in the 8880. A master-trigger of 1 V rectangle pulse from the infiTOF is used and introduced to a digital delay/pulse generator (Model 575, Berkeley Nucleonics Corporation, USA). The Model 575 converts to a transistor-transistor-logic pulse from the master-trigger and outputs to the digital multimeter NI PXIe-6361. Trigger synchronization among the converted master-trigger and PXI modules is performed using real-time system integration in the backplane of the NI PXIe-1082 chassis.

The noise characteristics of the iCD system are evaluated by a blank spectrum, which is produced by the same data acquisition procedure as the normal infiTOF operation[9] without the extraction of ions from the EI source. The baseline of the iCD spectrum is modulated by switching pulse noises derived from the rising and falling voltages of the entrance and exit deflection electric sectors of MULTUM-S II (Figure 3). To remove the modulation, a ± 48 ns moving average was applied to the blank iCD spectrum. The moving average was repeated 20 times. The moving average spectrum was subtracted from the blank iCD spectrum. The standard deviations of the noise signals decrease theoretically with increasing accumulation of the blank iCD spectrum with a slope to the power of ~ −0.5 (Figure 4). For an iCD spectrum, the estimated noise signal is 1000 ions, while for iCD spectra obtained after 10^8 accumulations, the estimated noise signal is ~0.3. This indicates that after 10^8 accumulations, single-ion detection with three standard deviation reliability is obtained. Thus, a dynamic range of this system is estimated to ~3×10^4 because ~10^4 ions from the ion source can be extracted for single mass scan and the minimum noise level is ~0.3 ion.

4. Experimental method

N$_2$ and perfluorotributylamine (PFTBA, molecular weight: 671) gases are used.

87　N₂ gas is introduced into the EI ion source of the infiTOF with He as the carrier gas. In

88　the case of PFTBA, the vaporized gas is directly introduced into the ion source. The

89　pressure in the ionization chamber is set to ~1×10^{-2} Pa during the measurements. The

90　ion packet produced in the ion source is introduced into the ion trajectory of the

91　MULTUM-S II using an entrance electric sector (Figure 1a). The voltage of the entrance

92　electric sector drops to the ground potential before the ions return to the sector. The signals

93　from ion packets during multiturning are detected by the iCD system. After multiturning,

94　the ion packets are output using an exit electric sector and detected by an electron

95　multiplier (EM) (148006 Fast-TOF Plus, ETP Ion Detect Pty Ltd., Australia).

96

97　**5. Data reduction procedure**

98　**5.1. Baseline correction**

99　　　　Figure 5 shows the iCD spectrum of the N₂–He gas mixture measured 2.4×10^{6}

100　times and averaged. Random noise levels of the accumulated spectrum correspond to 0.61

101　μV or 0.95 ions as standard deviation (Figure 4).

102　　　　The baseline of the iCD spectrum is modulated by the entrance pulses, as

103　discussed in Section 3 (Figure 5). The modulations of the baseline are removed in the

104　following steps: (1) selecting ion signals from the iCD spectrum using a differential filter

105　(Figures 6a₁, 6a₂, and 6b). Absolute ion intensities larger than the noise level in Figure 6b

106　are defined as peaks of ion signals. The standard deviation described above (0.95 ions)

107　was used as the noise level. Each peak of ion signals is defined as ± 58 ns outward from

108　the boundary between the peak profile and the noise level. The time width is determined

109　by the peak widths of several high peak profiles. The ion and noise signals are shown in

110　yellow and black, respectively (Figure 6c). (2) Ion signals from the differential iCD

111　spectrum are removed from the iCD spectrum. The removed areas are interpolated

112　linearly between both ends of the remaining data (Figure 6d). (3) To obtain the modulated

113　baseline profile, a ± 48 ns moving average is applied to the interpolated spectrum 20 times

114　(Figure 6e as a baseline profile of Figure 6a₂). (4) The baseline profile is subtracted from

115　the iCD spectrum (Figures 6f₁ and 6f₂). The baseline-corrected iCD spectrum is shown in

116　Figure 7.

117

118　**5.2. Convolution of iCD mass spectrum with autocorrelation function**

119　　　　An ion packet of *m/z* periodically passes through the iCD with a lap time of τ.

120　The autocorrelation function shown below converts the baseline-corrected iCD spectrum

121　into a mass spectrum: A function $f(\tau, t)$ that defines the ion packet $C(\tau)$ is denoted as the

122　conditional series sum of $Q(i\tau)$, which is the charge of an ion packet for each lap.

123 $$f(\tau,\ t) = \Sigma\, Q(\tau,t)\, g(\tau,t) = \sum_{i=1}^{n} Q(i\tau,t)\frac{1}{n}\qquad\qquad(1)$$

124 where t is a variable of TOF, and i is the multiturn number.

125   At time $t = t_a$,

126 $$g(\tau,t) = \begin{cases} 0 \ (Q(i\tau,t_a) < -V_{dis}) \\ 1 \ (Q(i\tau,t_a) \geq -V_{dis}) \end{cases}\qquad\qquad(2)$$

127 where V_{dis}, discrimination voltage between peaks and noise, is based on the noise level of

128 the iCD spectrum. This operation removes noise signals from the iCD spectrum. The

129 standard deviation of the noise of the measurement condition was set at $V_{dis} = 0.6\ \mu V$.

130 Furthermore, we set $Q((i+1)\,\tau,\,t_a) = Q(i\tau,\,t_a)$ if $Q((i+1)\,\tau,\,t_a)$ is greater than $Q(i\tau,\,t_a)$.

131 This operation removes the contribution of the overlapping ion peaks in the iCD spectrum.

132 Then, $C(\tau)$ can be expressed by the following equation:

133 $$C(\tau) = \int f(\tau,t)dt\qquad\qquad(3)$$

134 Expanding this expression, we get the following equation:

135 $$C(\tau) = \int_{-\Delta t}^{\Delta t}\frac{1}{n}\{Q(\tau + t_0 + t) + Q(2\tau + t_0 + t) + \cdots + Q(n\tau + t_0 + t)\}dt\qquad(4)$$

136 where t_0 is the TOF of the ion packet from the exit slit of the ion source to the iCD, which

137 is proportional to τ depending on the m/z, i.e., $t_0 = 0.3781\ \tau$. The coefficient 0.3781 is a

138 unique constant for the MULTUM-S II. Δt is the value that complements to t_0. We set Δt

139 $= 288$ ns, which is nearly twice the peak width of the iCD spectrum (Figure 7b). A larger

140 Δt provides a higher redundancy for the calculation but are computationally expensive.

141   A convolution from the iCD spectrum to the mass spectrum is calculated as $C(\tau)$

142 over a range of τ_{min} to τ_{max} in s_τ increments. The τ_{min} and τ_{max} are determined from the

143 mass spectrum obtained using MULTUM-S II operated in the half-cycle mode.[9] The s_τ

144 corresponds to the resolution of the m/z axis. We set $s_\tau = 0.5$ ns to derive a mass spectrum

145 of appropriate mass resolution. The m/z is calculated from τ if we use one or more internal

146 mass references.

147   Figure 8 shows the mass spectrum of the N_2−He gas mixture convolved using

148 Equation (4) from the iCD spectrum, as shown in Figure 7a. The m/z is calculated using

149 the ^{4}He and $^{28}N_2$ signals as internal mass references. The largest ion intensity among the

150 ions is in the mass spectrum with $^{28}N_2{}^+$ as the sample gas, and the second largest is in the

151 spectrum with ^{4}He$^+$ as the carrier gas. We observed $^{14}N^{15}N^+$ of the N_2 isotopologue and

152 $^{14}N^+$ as fragment ion of N_2. Peaks of $H_2{}^{16}O^+$, $^{32}O_2{}^+$, and $^{40}Ar^+$ were also detected, which

153 were from the residual air in the ion source.

154

155 **5.3. Mass resolving power of the convolved mass spectrum**

156   Given an ion packet at i laps of the iCD spectrum, the MRP of the ion packet
157 peak, MRP_{iCD} is calculated as:

158
$$MRP_{iCD}(i) = \frac{i\tau}{2\Delta T_i} = \frac{iL}{2l_{iCD}} \tag{5}$$

159 where ΔT_i is the full half-width maximum of the ion peak at i laps, L is the flight pass
160 length for one lap, and l_{iCD} is the length of the iCD tube. The L and l_{iCD} for MULTUM-S
161 II are 0.65 m and 0.018 m, respectively.
162   According to Equation (5), the MRP_{iCD} of N_2^+ increases linearly with increasing
163 i (Figure 9). The MRP of the convolved mass spectrum, MRP_{conv} calculated from Figure
164 8 also increases linearly with increasing i, but the slope is one-third of the slope of MRP_{iCD}
165 because of averaging the iCD N_2 peaks. This indicates that the MRP performance
166 improves if we combine the convolved mass spectrum and ion peaks extracted from the
167 iCD spectrum.
168

169 **6. Extended convolution using iCD and multiturn TOF spectra (Extended convolved**
170 **mass spectrum)**
171   To overcome the lower MRP performance of the convolved mass spectrum, we
172 applied a combination analysis between the iCD and the conventional EM ion detector.
173 Therefore, we used the experimental results of PFTBA because the characteristics of the
174 mass spectrum of PFTBA have been well studied and widely used for the mass calibration
175 of EI mass spectrometry.[14]
176   The multiturn TOF spectrum of PFTBA measured using the EM detector is
177 shown in Figure 10. The convolved mass spectrum calculated from the simultaneously
178 measured iCD spectrum is shown in Figure 11. In this calculation, we set $V_{dis} = 0$ V instead
179 of 0.6 µV to reject small ion signals close to noises.
180   We combined the convolved mass spectrum and multiturn TOF spectrum to
181 formulate an extended convolved mass spectrum. To replace the peaks of the convolved
182 mass spectrum with the peaks of the multiturn TOF spectrum, Equation (4) is changed to:
183
$$C(t) = I_{EM}(n\tau + t_0 + t_{ex}) \tag{6}$$
184 where I_{EM} is the ion intensity of the multiturn TOF spectrum at $(n\tau + t_0 + t_{ex})$. t_{ex} is the
185 TOF from the iCD to the EM detector to extract from the multiturn trajectory and is given
186 as:
187
$$t_{ex}(m/z) = t_a(m/z)^{1/2} + t_b \tag{7}$$
188 where t_a and t_b are constants given by the MS conditions (acceleration, toroidal sector
189 electric fields, and MATSUDA plate voltages). In this study, we determined t_a and t_b using
190 internal mass references at m/z 68.9952 (CF_3^+) and 218.9856 ($C_4F_9^+$). Using Equation (6),

191   we replaced the peaks appearing in Figure 11 with those appearing in Figure 10 to

192   construct an extended convolved mass spectrum of PFTBA (Figure 12). We compared the

193   peaks at m/z 130.9920 ($C_3F_5^+$) in the mass spectra (Figure 13). The MRP of the extended

194   convolved mass spectrum is the fully performed multiturn ion trajectory of the

195   MULTUM-S II.

196   The TOF of a peak of ion x on the multiturn TOF spectrum, T_x is expressed as:

197    $$T_x = \frac{n_x L + l}{v_x} \tag{8}$$

198   where n_x is the number of multiturn laps of ion x at extraction, l is the flight pass length

199   for half-cycle mode operation, and v_x is the flight speed of ion x. The flight pass lengths

200   are independent of ion x. From the peaks of ions x and y, we get:

201    $$\frac{v_x}{v_y} = \sqrt{\frac{m_y}{m_x}} \tag{9}$$

202   where m_i and m_j are the masses of the ions x and y, respectively. Then, L and l are

203   expressed as:

204    $$L = \frac{T_x v_x - T_y v_y}{n_x - n_y} = \frac{T_x - T_y \sqrt{\frac{m_x}{m_y}}}{n_x - n_y} v_x = \tau_x v_x \tag{10}$$

205    $$l = v_x(T_x - n_x \tau_x) \tag{11}$$

206   where τ_x is the lap time of ion x. Therefore, if ions x and y are used as internal references,

207   the T_z for ion z is calculated as:

208    $$T_z = (\tau_x(n_z - n_x) + T_x)\sqrt{\frac{m_z}{m_x}} \tag{12}$$

209    $$m_z = m_x T_z^2 (\tau_x(n_z - n_x) + T_x)^{-2}. \tag{13}$$

210   The measured masses m_z on the extended convolved mass spectrum were calculated from

211   Equation (13) using two internal mass reference peaks of CF_3^+ and $C_4F_9^+$. The molecular

212   formulas, exact masses, measured masses, mass differences, mass accuracies, number of

213   laps, and MRPs for PFTBA fragment ions are summarized in Table 1. The mass

214   accuracies are less than 80 ppm. The root mean square of the mass accuracies of the

215   system is 28 ppm. The value 28 ppm corresponds to the modulation amplitude of the

216   power supply because modulation causes fractionations of the lap time of ions by voltage

217   modulations of the electric sectors.[8]

218

219   **7. Conclusions**

220   We developed an iCD system to obtain mass spectra in a non-destructive mode.

221   We also formulated an autocorrelation function for this system to resolve the overtaking

222   problem in the multiturn TOF–MS. The iCD system provides m/z assignments of flying

223   ions along the multiturn trajectory. A mass spectrum was constructed from the iCD

224   spectra. An MRP of up to ~30,000 and mass accuracy of tens of ppm have been realized

225   by the iCD system installed in the MSI infiTOF.

226

230   References

231   1.   Ishihara M, Toyoda M, Matsuo T. Perfect space and time focusing ion optics for
232   multiturn time of flight mass spectrometers. *Int J Mass Spectrom.* 2000;197(1-
233   3):179-189. doi.org/10.1016/S1387-3806(99)00244-4

234   2.   Matsuo T, Ishihara M, Toyoda M, Ito H, Yamaguchi S, Roll R, Rosenbauer H. A
235   space time-of-flight mass spectrometer for exobiologically-oriented applications.
236   *Adv Space Res.,* 1999;23(2):341-348. doi.org/10.1016/S0273-1177(99)00055-1

237   3.   Toyoda M, Ishihara M, Yamaguchi S, Ito H, Matsuo T, Roll R, Rosenbauer H.
238   Construction of a New Multi-turn Time-of-Flight Mass Spectrometer. *J Mass
239   Spectrom.*   2000;35(2):163-167.   DOI: 10.1002/(SICI)1096-
240   9888(200002)35:2<163::AID-JMS924>3.0.CO;2-G

241   4.   Toyoda M, Okumura D, Yamaguchi S, Ishihara M, Katakuse I, Matsuo T.
242   Development of a multi-turn time-of-flight mass spectrometer 'MULTUM Linear
243   plus'.   *J   Mass   Spectrom   Soc   Jpn.*   2000;48(5):312-317.
244   doi.org/10.5702/massspec.48.312

245   5.   Toyoda M, Okumura D, Ishihara M, Katakuse I. Multi-turn time-of-flight mass
246   spectrometers with electrostatic sectors. *J Mass Spectrom.* 2003;38(11):1125-1142.
247   doi.org/10.1002/jms.546

248   6.   Okumura D, Toyoda M, Ishihara M, Katakuse I. A simple multi-turn time of flight
249   mass spectrometer 'MULTUM II'. *J Mass Spectrom Soc Jpn.* 2003;51(2):349-353.
250   doi.org/10.5702/massspec.51.349

251   7.   Okumura D, Toyoda M, Ishihara M, Katakuse I. Application of a multi-turn time-
252   of-flight massspectrometer, MULTUM II, to organic compounds ionized by matrix-
253   assisted laser desorption/ionization. *J Mass Spectrom.* 2004;39(1):86-90, 2004.
254   DOI: 10.1002/jms.575

255   8.   Tonotani A, Bajo K, Itose S, Ishihara M, Uchino K, Yurimoto H. Evaluation of
256   multi-turn time-of-flight mass spectrum of laser ionization mass nanoscope. *Surf
257   Interface Anal.* 2016;48(11):1122-1126. doi.org/10.1002/sia.6112

258   9.   Shimma S, Nagao H, Aoki J, Takahashi K, Miki S, Toyoda M. Miniaturized high-
259   resolution time-of-flight mass spectrometer MULTUM-S II with an infinite flight
260   path. *Anal Chem.* 2010;82(20), 8456-8463, 2010. doi.org/10.1021/ac1010348

261   10.   Shimma S, Nagao H, Giannakopulos AE, Hayakawa S, Awazu K, Toyoda M. High-
262   energy collision-induced dissociation of phosphopeptides using a multi-turn
263   tandem time-of-flight mass spectrometer 'MULTUM-TOF/TOF'. *J Mass Spectrom.*
264   2008;43(4):535-537. DOI: 10.1002/jms.1352

265   11.   Shimma S, Miki S, Toyoda M. Polychlorinated biphenyls (PCBs) analysis using a

266   miniaturized high-resolution time-of-flight mass spectrometer "MULTUM-S II". *J*
267   *Environ Monit*. 2012;14(6):1664-1670. doi.org/10.1039/C2EM30112A

268   12.   Shimma S, and Toyoda M. In *Greenhouse Gases - Emission, Measurement and*
269   *Management*, (Ed: G. Liu) 2012; Intech Open, London. pp. 235–254. doi:
270   10.5772/33815

271   13.   Bajo K, Fujioka O, Itose S, Ishihara M, Uchino K, Yurimoto H. Electronic data
272   acquisition and operational control system for time-of-flight sputtered neutral mass
273   spectrometer. *Surf Interface Anal.* 2019; 51(1): 35-39. doi.org/10.1002/sia.6541

274   14.   NIST Standard Reference Database 69: NIST Chemistry WebBook,
275   https://doi.org/10.18434/T4D303

276

277
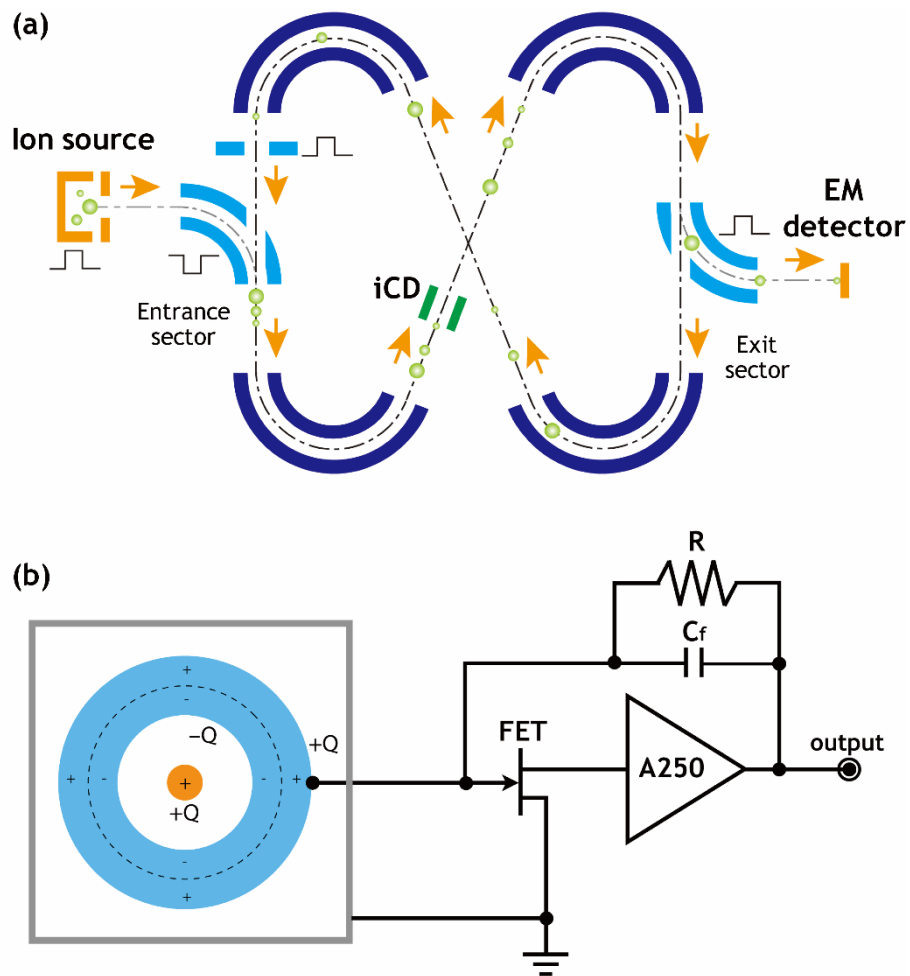
278
279 Figure 1. (a) Schematic of electrostatic-induced charge detector (iCD) installed in
280 MULTUM-S II and ion detection using a secondary EM detector (b) Schematic of charge
281 readout for ion packet charged +Q.
282

283
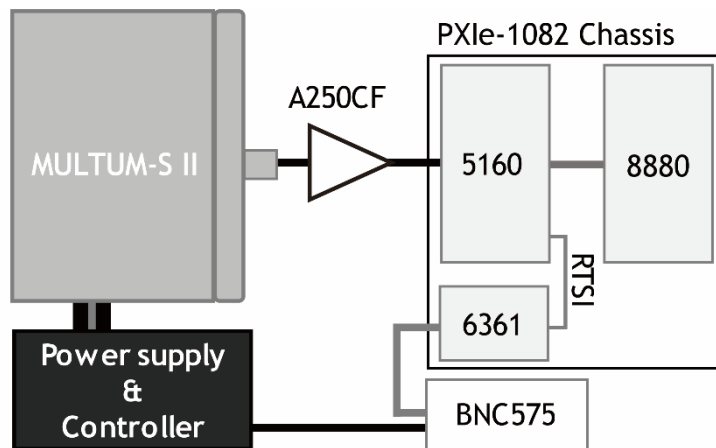
Figure 2. Schematic of data acquisition system for iCD. Outputs from A250CF preamplifier are converted to 10-bits digital signals using PXIe-5160 (5160) digitizer. The digital signals are processed and stored by PXIe-8880 (8880). BNC575 and PXIe-6361(6361) controls timing for data acquisition.

288
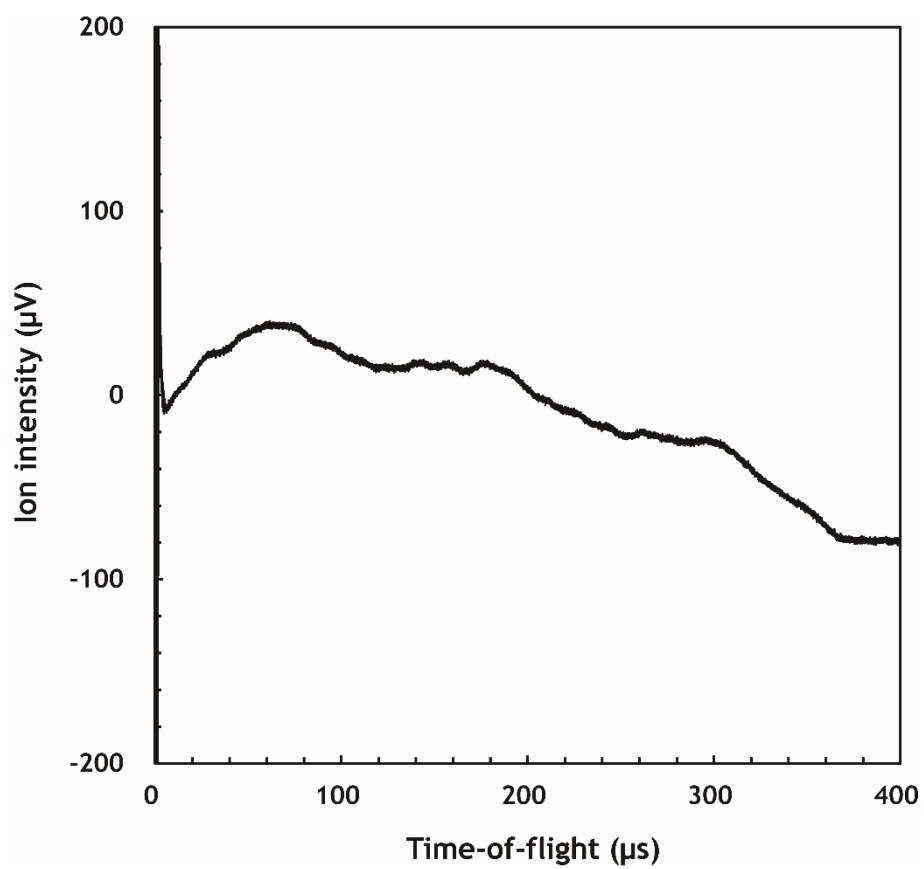
289
290 Figure 3. Baseline of an iCD spectrum, of which accumulation of the iCD spectra was
291 2.4×10^6.
292

293
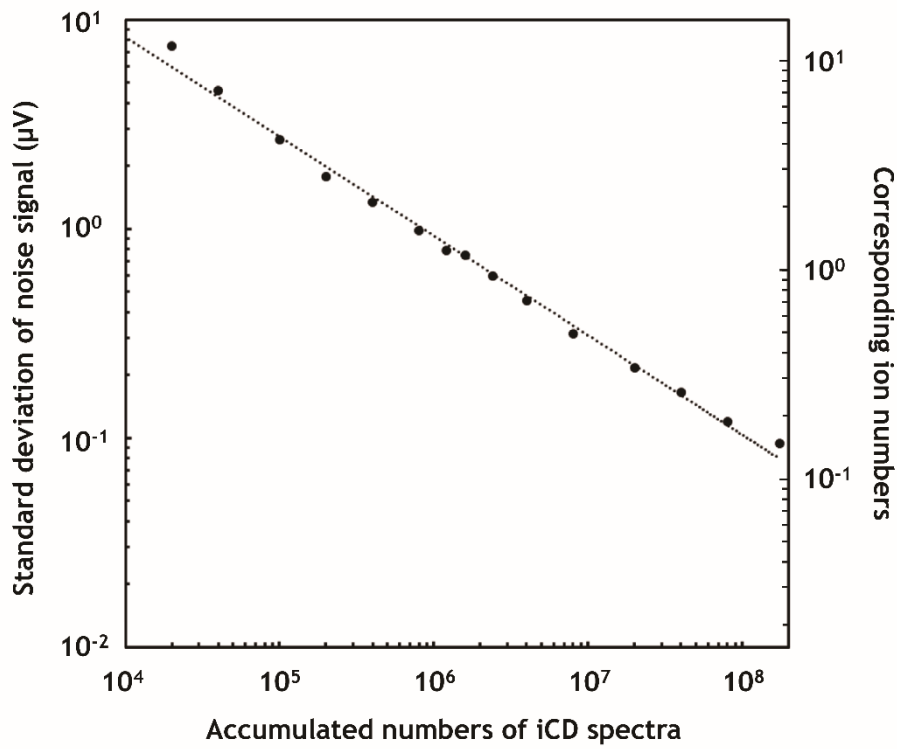
Figure 4. Standard deviations of noise signal as a function of accumulated numbers of
iCD spectra. Dotted line represents a power approximate expression (y (μV) = 664.0 $x^{-0.476}$).

297
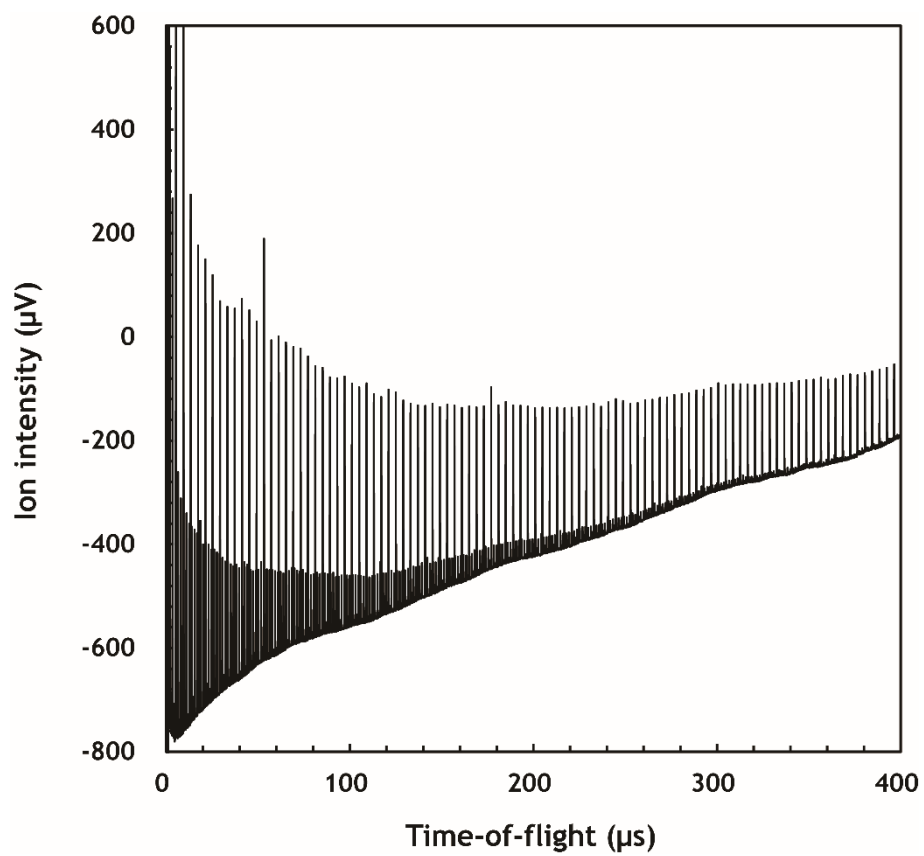
298

299 Figure 5. iCD spectrum of N_2–He gas.

300
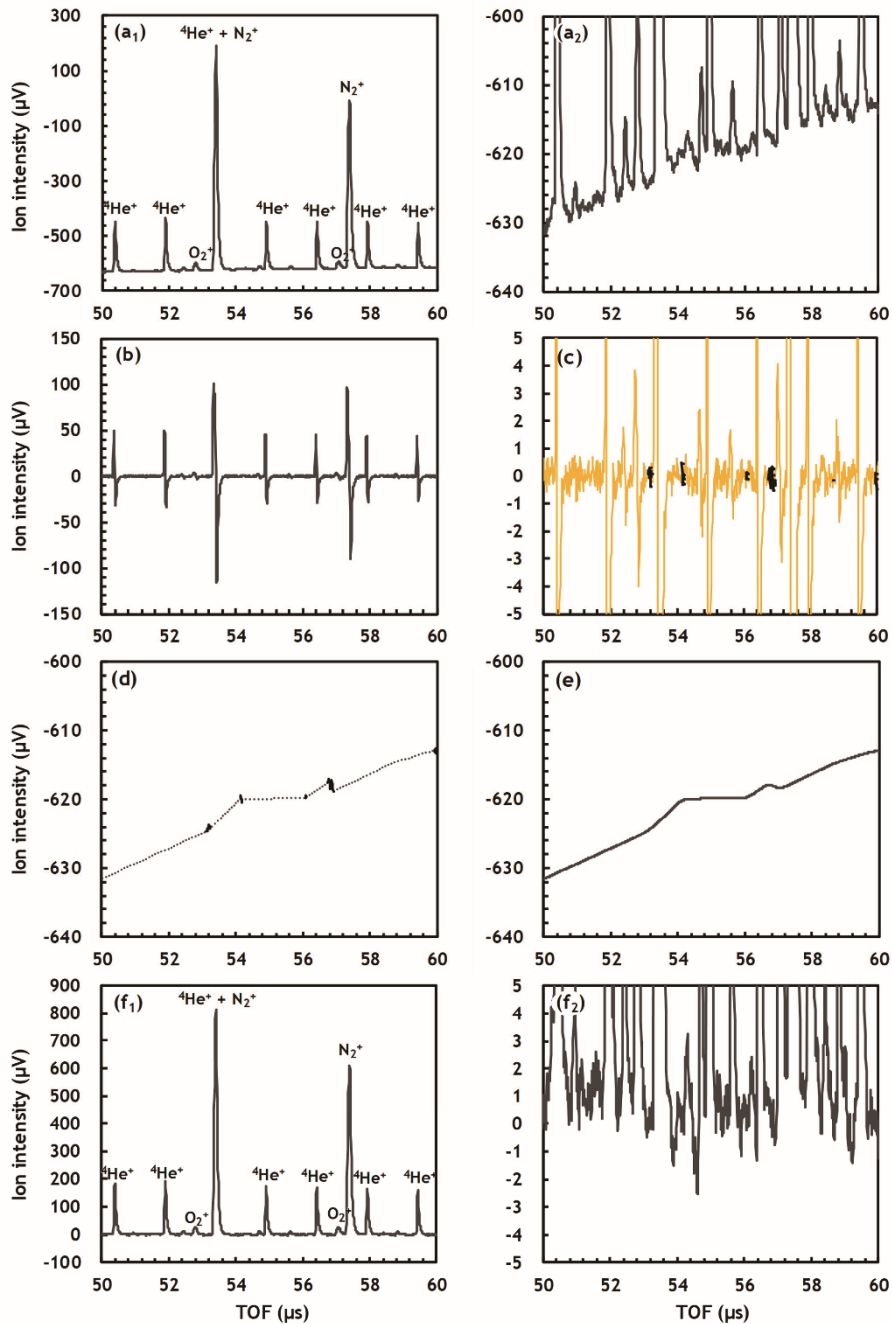
Figure 6. Procedure of baseline correction. (a_1) An enlarged iCD spectrum of Figure 5 (50 µs to 60 µs). (a_2) An enlarged iCD spectrum of the baseline of (a_1). (b) A differential iCD spectrum of (a_1). (c) An enlarged differential iCD spectrum of (b). Ion and noise signals are shown in yellow and black, respectively. (d) The noise signals of (c) are removed and interpolated linearly (dotted line). (e) Smooth profile of (d) as modulated baseline profile of (a_2). (f_1) A baseline-corrected iCD spectrum. Full spectrum is shown in Figure 7. (f_2) An enlarged baseline-corrected iCD spectrum of (f_1).
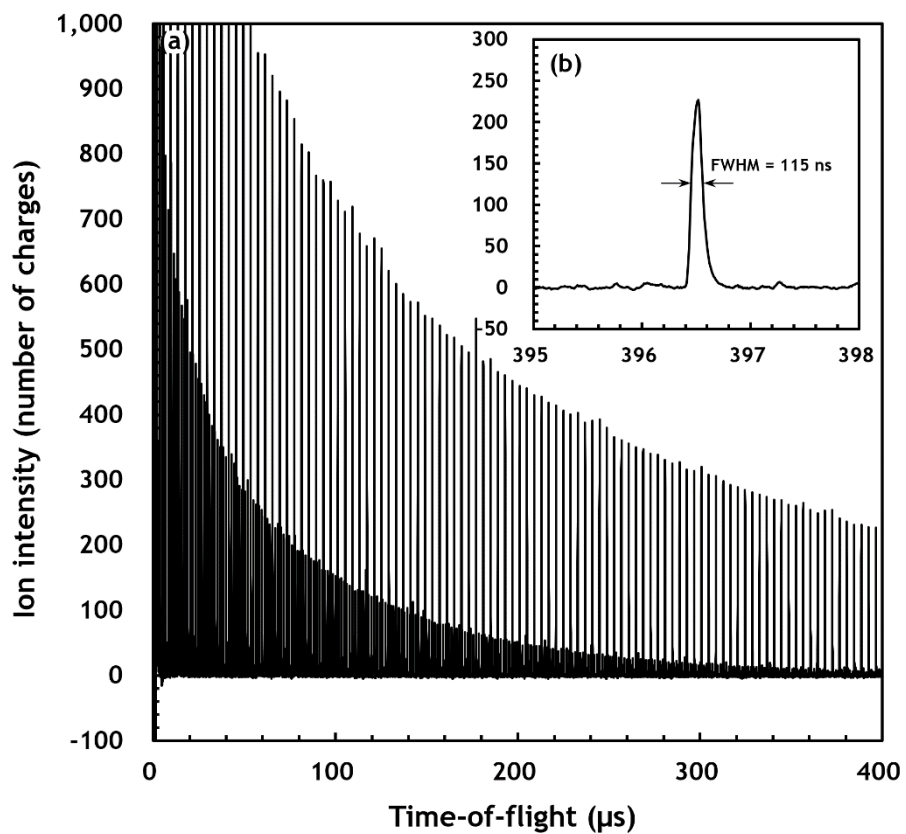
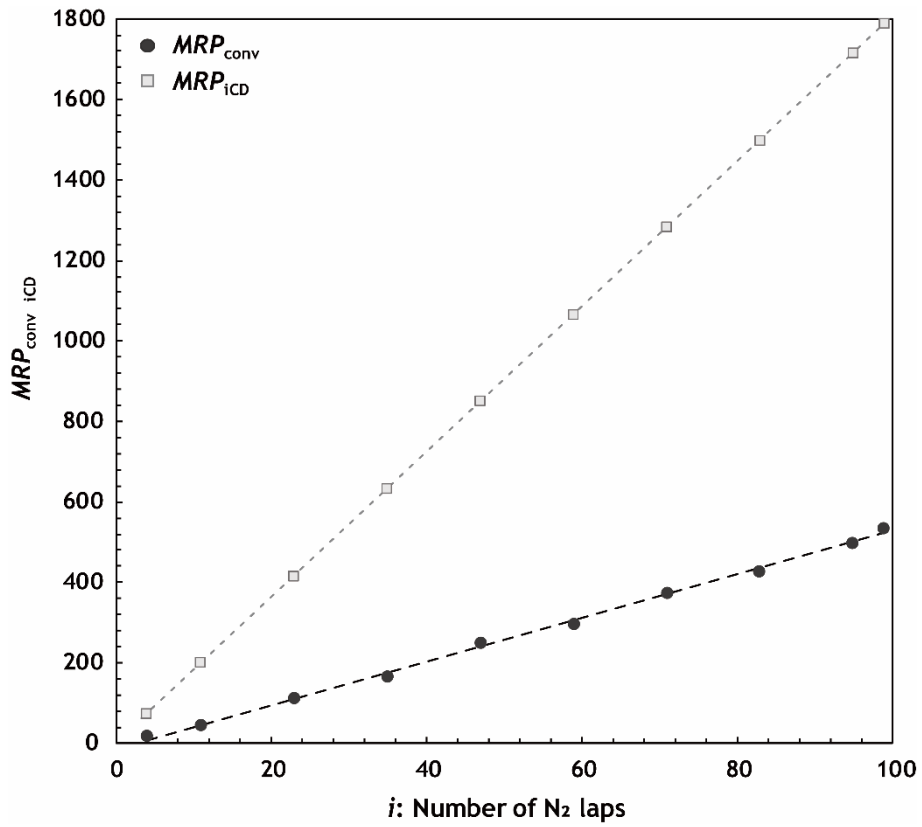Figure 7. (a) Baseline-corrected iCD spectrum of N$_2$–He gas. (b) A spectrum at 396.5 µs.
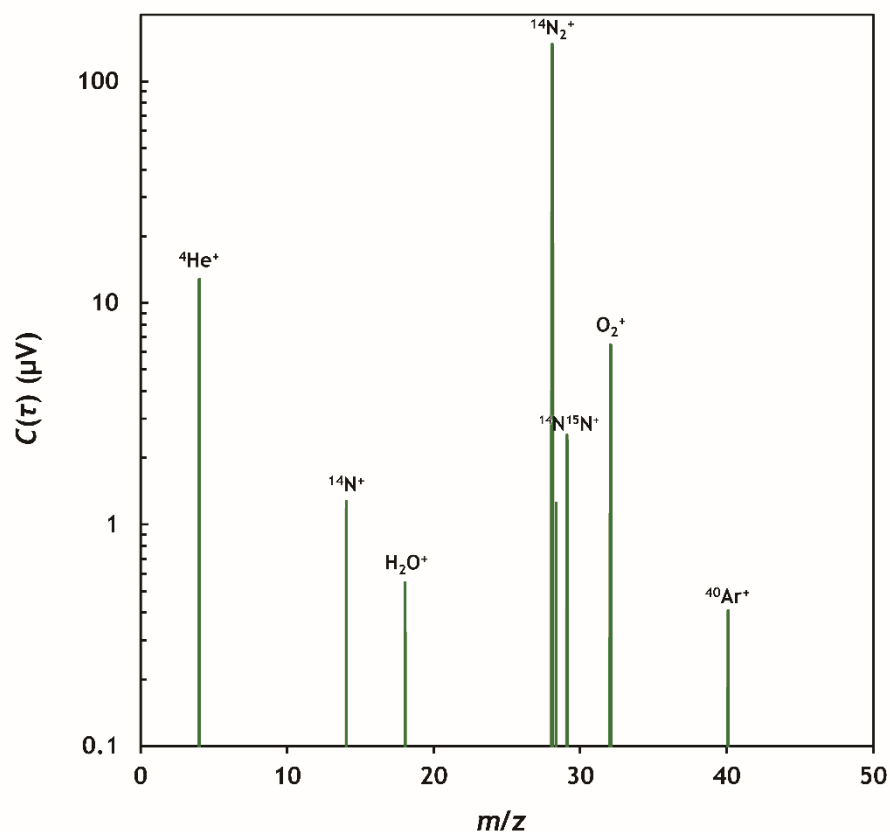
Figure 8. Convolved mass spectrum of N_2–He gas calculated from iCD spectrum. τ_{min}, τ_{max}, s_τ, t_0, Δt and V_{dis} were set at 0.96 μs, 4.80 μs, 0.5 ns, 0.3781 τ, 288 ns, and 0.6 μV, respectively. The m/z (horizontal axis) is calculated from τ using internal mass references at m/z 4.00260 ($^4He^+$) and 28.00615 ($^{28}N_2^+$).
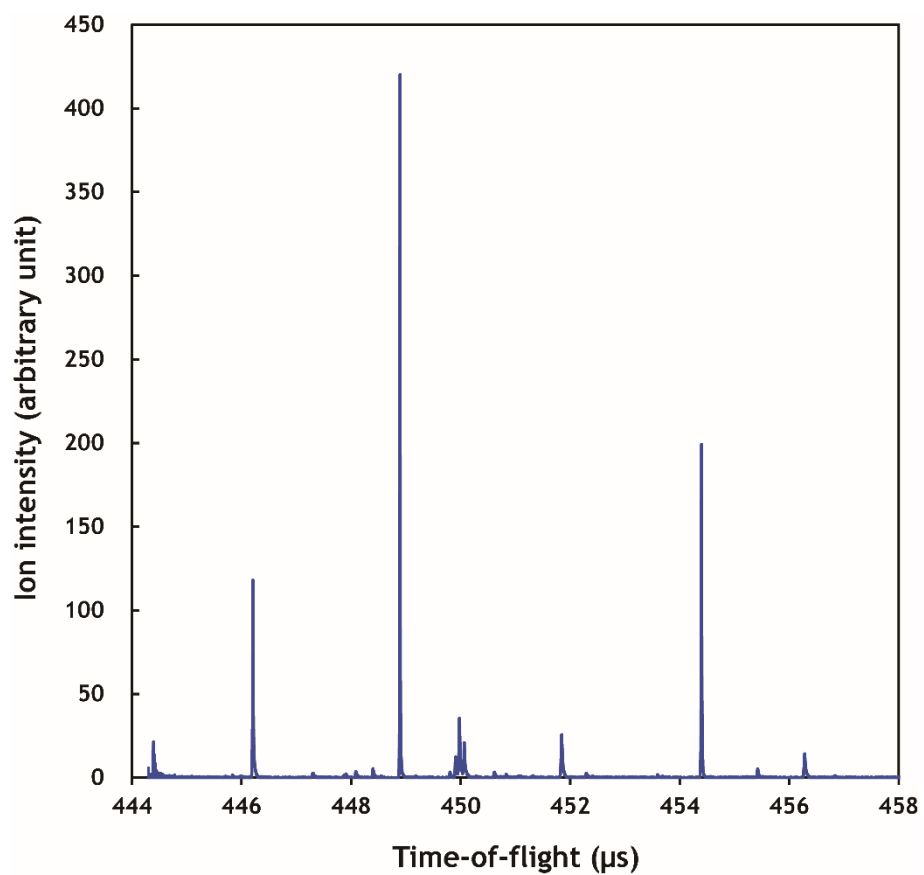
319

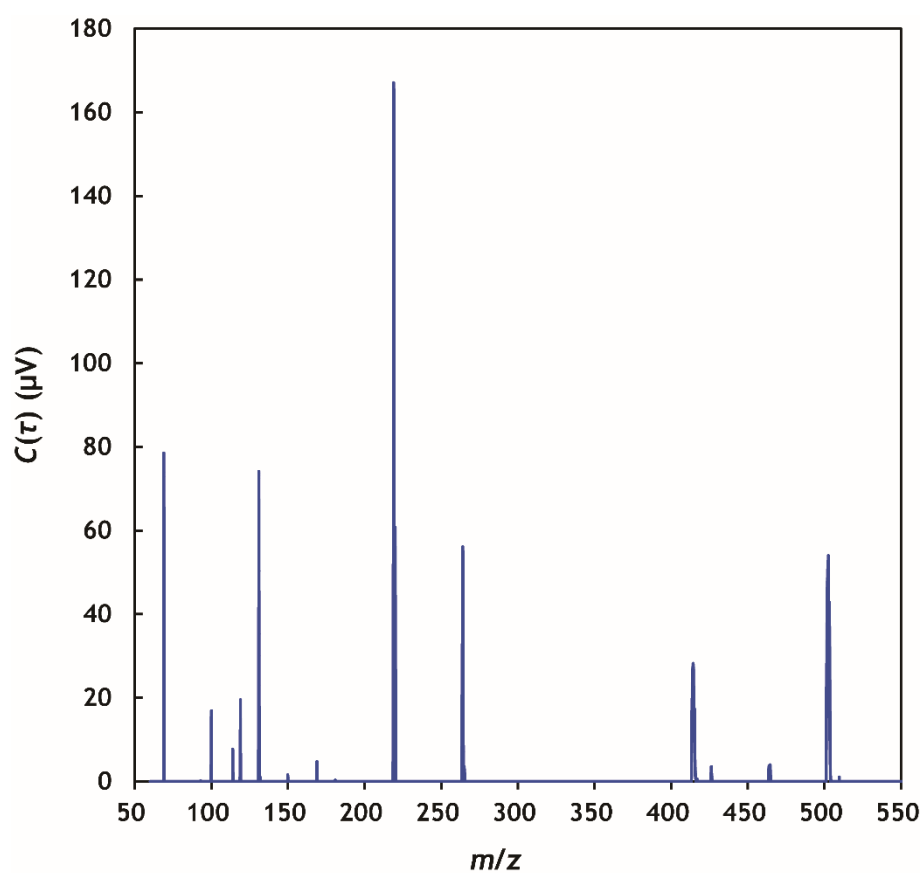Figure 9. Change of MRP_conv and MRP_iCD of N_2^+ as a function of number of multiturn
laps.

323

324   Figure 10. Multiturn TOF spectrum of PFTBA extracted from the multiturn trajectory.

325

Figure 11. Convolved mass spectrum of PFTBA calculated from iCD spectrum. τ_{min}, τ_{max}, s_τ, t_0, Δt and V_{dis} were set at 5.76 μs, 17.28 μs, 0.0638 ns, 0.3781 τ, 384 ns, and 0 V respectively. The m/z (horizontal axis) is calculated from τ using internal mass references of m/z 68.9952 (CF_3^+) and 218.9856 ($C_4F_9^+$).

332
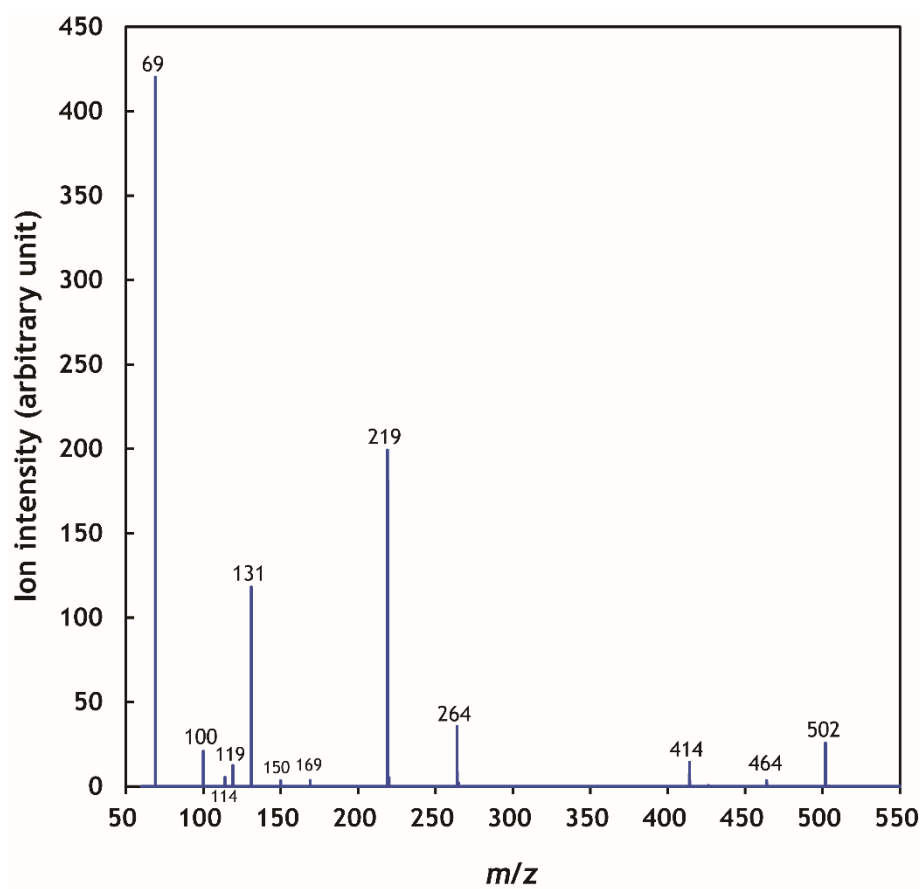
Figure 12. Extended convolved mass spectrum of PFTBA.

334
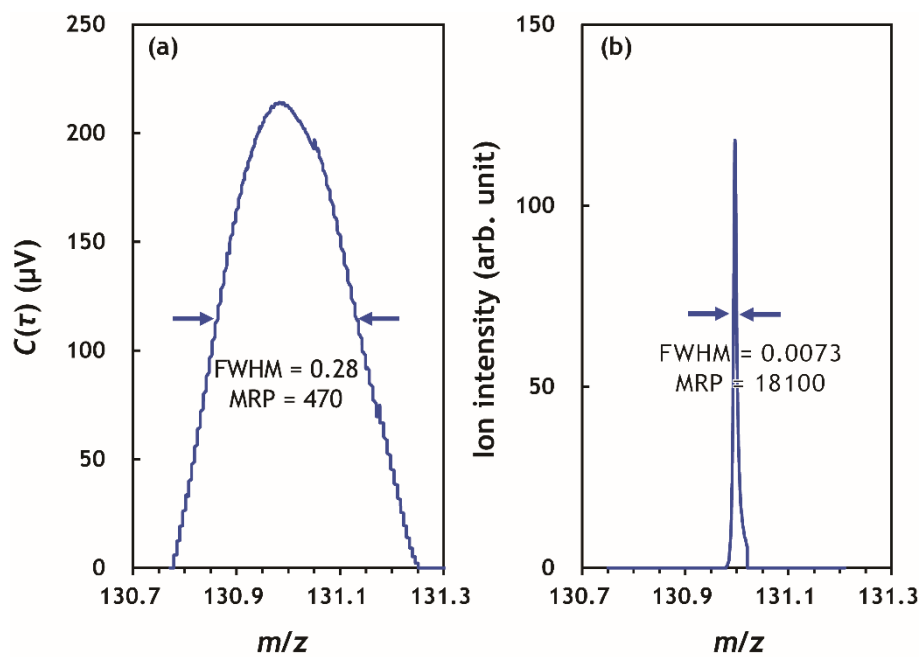
Figure 13. Peak shapes at *m/z* 130.9920 ($C_3F_5^+$) (a) from Figure 11, (b) from Figure 12.

338 Table 1. molecular formulas, exact masses, measured masses, mass differences (Δm),
339 mass accuracies, number of laps, and mass resolution (MRP) of major peaks from PFTBA
340 sample.

Molecular formula	Exact mass	Measured mass	Δm	Mass accuracy	Number of laps	MRP
			$\times 10^{-3}$	ppm		
CF_3	68.9952	68.9952	0.0	0	71	28200
C_2F_4	99.9936	99.9897	3.9	39	59	10800
$C_3F_4H_2$	113.9973	113.9926	4.7	42	55	9000
C_2F_5	118.9920	118.9876	4.4	37	54	10800
C_3F_5	130.9920	130.9897	2.4	18	51	18100
C_3F_7	168.9888	168.9797	9.1	54	45	7300
C_4F_9	218.9856	218.9856	0.0	0	40	20500
C_4F_9H	219.9935	219.9752	18.3	83	40	10300
C_5NF_{10}	263.9877	263.9807	7.1	27	36	9600
$C_5NF_{10}H$	264.9956	265.0001	−4.5	17	36	9800
C_8NF_{16}	413.9782	413.9701	8.1	20	29	8700
C_9NF_{18}	463.9750	463.9589	16.1	35	27	6900
C_9NF_{20}	501.9718	501.9678	4.0	8	26	8500

341